Article

Antibacterial Electrospun PVA/Enzymatic Synthesized Poly(catechol) Nanofibrous Mid-Layer Membrane for Ultrafiltration

Dora Coelho, Ana Sampaio, Carla J S M Silva, Helena P. Felgueiras, M. Teresa P. Amorim, and Andrea Zille

Just Accepted

Antibacterial Electrospun PVA/Enzymatic Synthesized Poly(catechol) Nanofibrous Mid-Layer Membrane for Ultrafiltration

Dora Coelho[‡], Ana Sampaio[‡], Carla J. S. M. Silva[‡], Helena P. Felgueiras[†], M. Teresa P. Amorim[†] and Andrea Zille[†]*

[‡]Centro de Nanotecnologia e Materiais Técnicos, Funcionais e Inteligentes (CeNTI), 4760-034 Vila Nova de Famalicão, Portugal.

[†]2C2T - Centro de Ciência e Tecnologia Têxtil, Universidade do Minho, Campus de Azurém, 4800-058 Guimarães, Portugal.

KEYWORDS: poly(vinyl alcohol), catechol, silver nitrate, electrospinning, membrane, water filtration.

ABSTRACT: Two different nanofibrous antibacterial membranes containing enzymatically synthesized poly(catechol) (PC) or silver nitrate ($AgNO_3$, positive control) blended with poly(vinyl alcohol) (PVA) and electrospun onto a poly(vinylidene fluoride) (PVDF) basal disc to generate thin-film composite mid-layers were produced for water ultrafiltration applications. The developed membranes were thoroughly characterized in terms of morphology, chemical composition and general mechanical and thermal features, antimicrobial activity and ultrafiltration capabilities. The

electrospun blends were recognized as homogeneous. Data revealed relevant conformational changes in the PVA side groups, attributed to hydrogen bonding, and high thermal stability and residual mass. PVDF+PVA/AgNO$_3$ membrane displayed 100% growth inhibition of both Gram-positive and Gram-negative bacteria strains, despite the wide range of fiber diameters generated, from 24 to 125 nm, formation of numerous beads and irregular morphology. The PVDF+PVA/PC membrane showed a good growth inhibition of *Staphylococcus aureus* (92%) and revealed a smooth morphology, with no relevant bead formations and diameters ranging from 68 to 131 nm. The ultrafiltration abilities of the membrane containing PVA/PC were tested in a dead-end high-pressure cell (4 bar) using a reactive dye in distilled water and seawater. After 5 cycles, a maximum rejection of $\approx$ 85% with an average flux rate of 70 L m^{-2} h^{-1} for distilled water and $\approx$ 64% with an average flux rate of 62 L m^{-2} h^{-1} for seawater were determined with an overall salt rejection of $\approx$ 5%.

1. INTRODUCTION

Catechols are small colorless molecules usually applied for the synthesis of food, pharmaceuticals or agrochemical ingredients. They occur naturally in trace amounts in fruits or vegetables but can also be found in insects, teas and even poisons. Catechols are versatile electroactive species that undergo a variety of chemical reactions, and are capable of establishing interactions with both organic and inorganic substrates. Catechols possess a pivotal role as adhesive interfaces and effective anchoring groups, giving rise to a large range of polymeric materials with fascinating structures and properties.[1-2] Most importantly, catechols have shown to display antibacterial and antifungal effects against various microorganisms.[3-4]

2

1
2
3
4
5
6
7
8
9
10
11
12
13
14
15
16
17
18
19
20
21
22
23
24
25
26
27
28
29
30
31
32
33
34
35
36
37
38
39
40
41
42
43
44
45
46
47
48
49
50
51
52
53
54
55
56
57
58
59
60

For many years, the polymeric synthesis of phenol-derived compounds, including catechol, was a challenge and only accomplished through the conventional formaldehyde-based high-temperature process. Enzymatic polymerization has provided a new strategy for the synthesis of phenols and aromatic amine-based polymers.[5] Enzymatic polymerization is defined as "the *in vitro* polymerization of artificial substrate monomers catalyzed by an isolated enzyme via non biosynthetic (non metabolic) pathways".[1, 6] The enzymes laccase, lipase and peroxidase have been recognized as capable of catalyzing phenols, including catechol into poly(catechol) (PC).[7-10] This strategy possesses many advantages over conventional processes, as requiring only mild reaction conditions (e.g. temperature, pressure and pH) and being non-toxic.[5, 11-12] Although the literature has pointed some of the uses for PC,[1] its application in nanofibrous porous supports for thin-film composite (TFC) membranes for water ultrafiltration applications has not yet been exploited.

TFC asymmetric membranes are composed of a top selective layer and a bottom porous substrate that can be independently controlled and optimized to achieve desired selectivity and permeability, while offering excellent mechanical strength. Over the years, a large variety of polymers has been successfully used as porous supports for TFC membrane fabrication.[13] Poly(vinylidene fluoride) (PVDF), a fluorinated-derived polymer with great chemical, thermal, and mechanical stabilities, has been a material of choice. Still, the use of PVDF as support layers in TFC membranes comes with limitations, namely is its high surface hydrophobicity, which complicates adhesion of other materials on the surface.[14] Modification of the PVDF support layer is therefore recommended. In the present research, enzymatically synthesized PC blended with poly(vinyl alcohol) (PVA) were electrospun onto a PVDF basal membrane to overcome this limitation.

3

Electrospinning is broadly used for polymer fiber production of thinner diameters, from 2 nm to several micrometers.[15] It is a simple and straightforward method, in which a single polymer or polymeric blend is pumped at constant rate through a syringe or capillary tube connected to a high DC voltage source.[16-18] PVA membranes produced by electrospinning are very common. As a biodegradable, non-toxic or non-carcinogenic, biocompatible synthetic polymer with good mechanical properties, PVA is desirable for many applications.[19-22] Also, PVA can reduce the repulsive forces within the charged polymer solution to facilitate fiber electrospinning.[23] Its flexibility and swelling capability in aqueous environments are in particular cases of great interest, however may also represent a downside, affecting its stability. Blends of PVA with other polymers are, therefore, frequent.[24-26] Son et al. has shown PVA and catechol, oxidized and polymerized with amines in the form of polydopamine, to work in harmony to improve the electrospun surfaces stability as well as to increase binding of silver nanoparticles (Ag NPs) and, with that, the surface antimicrobial features.[27] To the authors knowledge, the PVA and PC potentialities have yet to be explored in the form of an ultra-thin and defect-free selective barrier for TFC membranes.

In the present investigation, PVDF basal membranes were electrospun with PVA/PC blends to generate a mid-layer nanofibrous porous support for TFC membranes used in water ultrafiltration applications. PC was synthesized by enzymatic polymerization catalyzed by laccase. This is the first time an enzymatically synthesized PC is used in the production of electrospun nanofibers. A nanofibrous antibacterial membrane containing silver nitrate ($AgNO_3$) blended with PVA was also produced and used as positive control. The two membranes were thoroughly characterized in terms of morphology, chemical composition and general mechanical and thermal features, using scanning electron microscopy (SEM), energy-dispersive X-ray spectroscopy (EDS), X-

1
2
3
4
5
6
7
8
9
10
11
12
13
14
15
16
17
18
19
20
21
22
23
24
25
26
27
28
29
30
31
32
33
34
35
36
37
38
39
40
41
42
43
44
45
46
47
48
49
50
51
52
53
54
55
56
57
58
59
60

ray photoelectron spectroscopy (XPS), dynamic mechanical analysis (DMA), thermogravimetry (TGA), and differential scanning calorimetry (DSC). The membrane antimicrobial properties were evaluated against *Escherichia coli* (*E. coli*) and *Staphylococcus aureus* (*S. aureus*) bacteria. The PVDF+PVA/PC ultrafiltration capabilities (e.g. flux) were established with distilled water (dH$_2$O) and synthetic seawater.

2. EXPERIMENTAL SECTION

2.1. Materials. PVA 87-90 % hydrolyzed (wt 30,000-70,000), AgNO$_3$ and catechol were purchased from Sigma Aldrich (USA), and the PVDF basal disc filter (5 cm in diameter and porosity of 0.02 μm) from Sterlitech (USA). Laccase from *Myceliophthora thermophila* (NS51003, Novozymes, Bagsvaerd, Denmark) was kindly provided by Professor Diego Moldes' Group from University of Vigo, Spain. Bacteria were acquired from the American Type Culture Collection (ATCC) company: *E. coli* (ATCC 25922) and *S. aureus* (ATCC 6538). The remainder materials were all purchased from Sigma-Aldrich and used without further purification.

2.2. Enzymatic Polymerization Catalyzed by Laccase. PC was obtained from a 50 mM catechol solution incubated with 5 mg of laccase at 0.5 U/mg. Polymerization reaction was carried out overnight in a stirring system (0.1 M acetate buffer, pH 5.0) at 50º C, as described in[28].

2.3. Electrospinning. The electrospinning experiments were performed in a Nanon NF-103 (MECC, Japan) at room temperature (RT), using a 10 mL syringe with a needle of 0.5 mm inner diameter. An electric field of 27 kV was applied to all solutions. The

feed rate was 0.2 mL/h. The nanofibres were deposited on a collecting plate at the controlled distance of 120 mm. The solutions viscosity and conductivity were measured using a viscometer (Fungilab Smart Series Rotational Viscometer) and a conductivimeter (Thermo Scientific), respectively. Solutions containing $AgNO_3$ were prepared in a 60/40 ratio of PVA (12%, w/w) and $AgNO_3$ (1.5%, w/w) in dH_2O, while the solution containing catechol was prepared by dissolving PVA (12%, w/w) directly in the enzymatically synthesized PC solution (60/40 ratio). The mixed solutions were electrospun onto a PVDF basal microfiltration disc filter. Since PVA has poor stability in water, the electrospun membranes were further cross-linked by glutaraldehyde (GA) to maintain its morphology and prevent dissolution. GA has two active sites and can promote intramolecular and intermolecular nonspecific bindings between PVA molecules, decreasing membranes hydrophilicity without the need of thermal treatment. Electrospun membranes were immersed in a 5 mM GA and 0.01 N HCl water solution for 6 h, washed several times, and kept in water until use.[29] After electrospinning, the porosity was calculated through the relationship between volume and density. The used equation was $P = (1-(\rho/\rho_0))$, where P is the porosity, ρ is the density of the electrospun membrane, and ρ_0 is the density of the bulk polymer.

2.4. Scanning Electron Microscopy (SEM) and Energy Dispersive X-ray Spectroscopy (EDS). Morphology analyses of the prepared nanofibres were carried out with an Ultra-High Resolution Field Emission Gun SEM, NOVA 200 Nano SEM, FEI Company. Secondary electron images were acquired with an acceleration voltage of 5 kV, while backscattering electron images were obtained with an acceleration voltage of 15 kV. To improve conductivity, the tested surfaces were covered with a film of Au-Pd (80-20 weight %) using a high-resolution sputter coater, 208HR Cressington Company, coupled to a MTM-20 Cressington high resolution thickness controller. The

membranes atomic compositions were examined with an EDS (coupled to the SEM

equipment) using an EDAX Si(Li) detector and an acceleration voltage of 5 kV.

2.5. X-Ray photoelectron spectroscopy (XPS). XPS measurements were performed

on a VG Scientific ESCALAB 200A equipment with PISCES software for data

acquisition and analysis. For analysis, an achromatic Al (Ka) X-ray source operating at

15 kV (300 W) was used, and the spectrometer, calibrated with reference to Ag 3d5/2

(368.27 eV), was operated in CAE mode with 20 eV pass energy. Data acquisition was

conducted with a pressure lower than 1E-6 Pa. Deconvolution into sub-peaks was

performed by least-squares peak analysis software, XPSPEAK version 4.1, using the

Gaussian/Lorenzian sum function and Shirley-type background subtraction (or linear

consideration of the data).

2.6. Thermogravimetric Analysis (TGA). TGA was carried out on a Pyris 1 TGA

(Perkin Elmer, USA) according to the standard ISO 11358:1997(E). The TGA trace was

obtained in the range of 40-900 °C under nitrogen atmosphere, with a flow rate of

20 mL/min and heating rate of 10 °C/min. Samples were dried at 60 °C for 1 h and

placed into a porcelain sample pan before analysis. Data was plotted as weight

(percentage) vs. temperature.

2.7. Differential Scanning Calorimeter (DSC) Analysis. DSC was carried out on a

Power compensation Diamond DSC (Perkin Elmer, USA) with an Intracooler ILP,

based on the standards ISO 11357-1:1997, ISO 11357-2:1999 and ISO 11357-3:1999.

Samples were dried at 60 °C for 1 h and placed in an aluminum sample pan before

testing. The analysis was carried out in nitrogen atmosphere with a flow rate of

20 mL/min and heating rate of 10 °C/min. The thermogram was obtained in the range of

-50 °C to -200 °C. This upper limit for DSC was selected since this was the temperature

7

in which all the tested polymers started decomposition, as seen by TGA. Data was plotted as heat flow vs. temperature.

2.8. Dynamic Mechanical Analysis (DMA). DMA analysis was performed on a DMA 8000 (Perkin Elmer, USA) in tension mode according to an internal method based on standard ASTM D4065-01. The temperature dependence of the storage modulus and loss tangent was measured from -50 to 120 °C at a 2 °C/min rate.

2.9. Antimicrobial Testing. The antimicrobial activity was assessed according to the standard shake flask method (ASTM-E2149-01). This method provides quantitative data for measuring the reduction rate in number of colonies formed, converted to the average colony forming units per milliliter of buffer solution in the flask (CFU/mL). *E. coli* (ATCC 25922) and *S. aureus* (ATCC 6538) were expanded from a single colony. The culture was then inoculated 24 h in sterile nutrient broth (NB, Sharlab, Spain) at 37 ºC and 230 rpm. The inoculated bacterial culture was harvested by centrifugation and washed twice with a 0.9 % solution of NaCl at pH 6.5. Thereafter, the samples were incubated with 5 mL of bacterial suspension (previously diluted 10 fold with NaCl 0,9 % pH 6.5) at 37 ºC and 100 rpm. For determination of the inoculum cell density the suspensions were withdrawn before contact with the sample and after 1 h contact. The withdrawn suspensions were serially diluted in sterile buffer solution, plated on a plate count agar (VWR) and further incubated at 37 ºC for 24 h to determine the number of surviving bacteria. Antimicrobial activity, defined by equation (1), was reported in terms of percentage of bacteria reduction calculated as the ratio between the number of surviving bacteria before and after the contact with the electrospun membranes:

Bacteria reduction (%)= $\left[\frac{A-B}{A}\right] \times$ 100,

(1)

where A and B are the average number of bacteria before and after the contact with the samples, respectively. All experiments were conducted in triplicate with data being only considered if the error between measurements was smaller than 15%.

2.10. Ultrafiltration. The ultrafiltration experiments were carried out at 25 °C using a C.I. Reactive Red 66 monoazo dye (0.1 g/L - 629.37 MW – λ max 570 nm) at 4 bar dispersed in 50 mL of dH_2O and synthetic seawater using the ASN-III$_0$ medium. The system consisted of a 300 mL bench stainless steel tangential flow stirred cell (Sterlitech, HP4750, active membrane area, 14.6 cm^2) pressurized with air. The solution in the chamber was stirred with a teflon-coated magnetic bar at 300 rpm. All membranes were preconditioned by filtering the solutions at 4 bar of pressure until a steady flux was guaranteed. At the end of filtration, the feed, permeate and retentate, were collected and the concentration and solute rejection were determined using UV/vis spectrophotometry. The membrane flux, defined as the volume of solvents and solutes that pass through the membrane unit area per unit time, was calculated dividing the volume of permeate by the membrane active area and filtration time. The overall salt rejection was calculated using a conductivimeter and expressed as percentage of reduction using the seawater mother solution as reference (44 mS cm^{-1}). A calibration curve was established using the UV/vis spectrophotometry. Each experiment was conducted in triplicate.

3. RESULTS

3.1. Membrane Characterization. The nanofibrous membranes morphology, chemical composition and general mechanical and thermal features were characterized using SEM, EDS, XPS, DMA, TGA and DSC techniques. SEM micrographs of the PVA, PVA/AgNO$_3$ and PVA/PC electrospun nanofibers onto the PVDF basal membrane were taken (Figure 1). Beads and discontinuous fibers within the PVA nanofibrous membranes were detected. Fibers were classified as heterogeneous in size varying between 36 and 147 nm, with an average diameter of $\approx$ 81 nm, and porosity of $\approx$ 88% (Table 1). Beads within the nanofibers produced from the PVA/AgNO$_3$ blend were very frequent. Here, the nanofibers diameter varied between 24 and 125 nm with a porosity of $\approx$ 90%. The integrity of the fibers was as well compromised, with discontinuous and very thin nanofibers being detected. To the contrary, very little beads and smooth nanofibers were observed using the PVA/PC blend. Nanofibers were relatively homogeneous in shape and diameter compared to the other blends; average diameter and porosity were established at $\approx$ 98 nm (69-131 nm) and 51%, respectively.
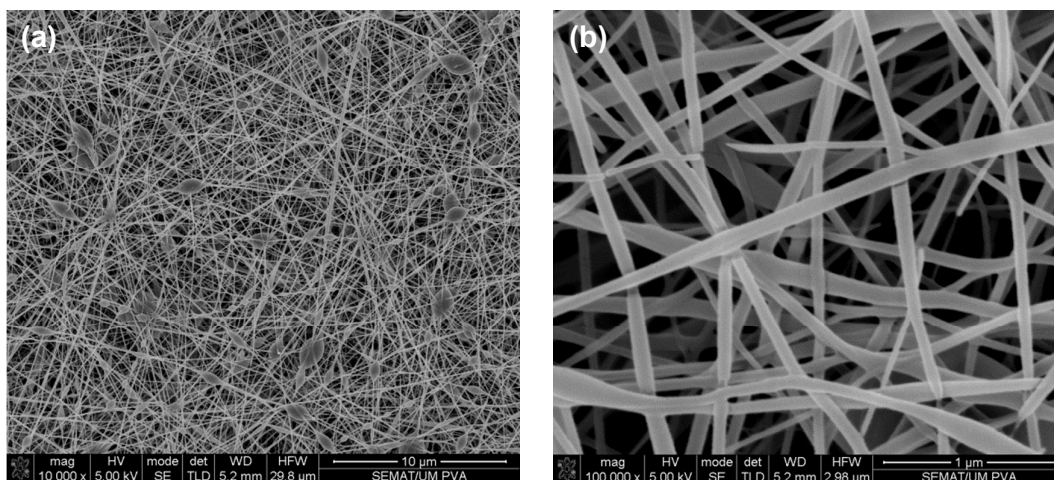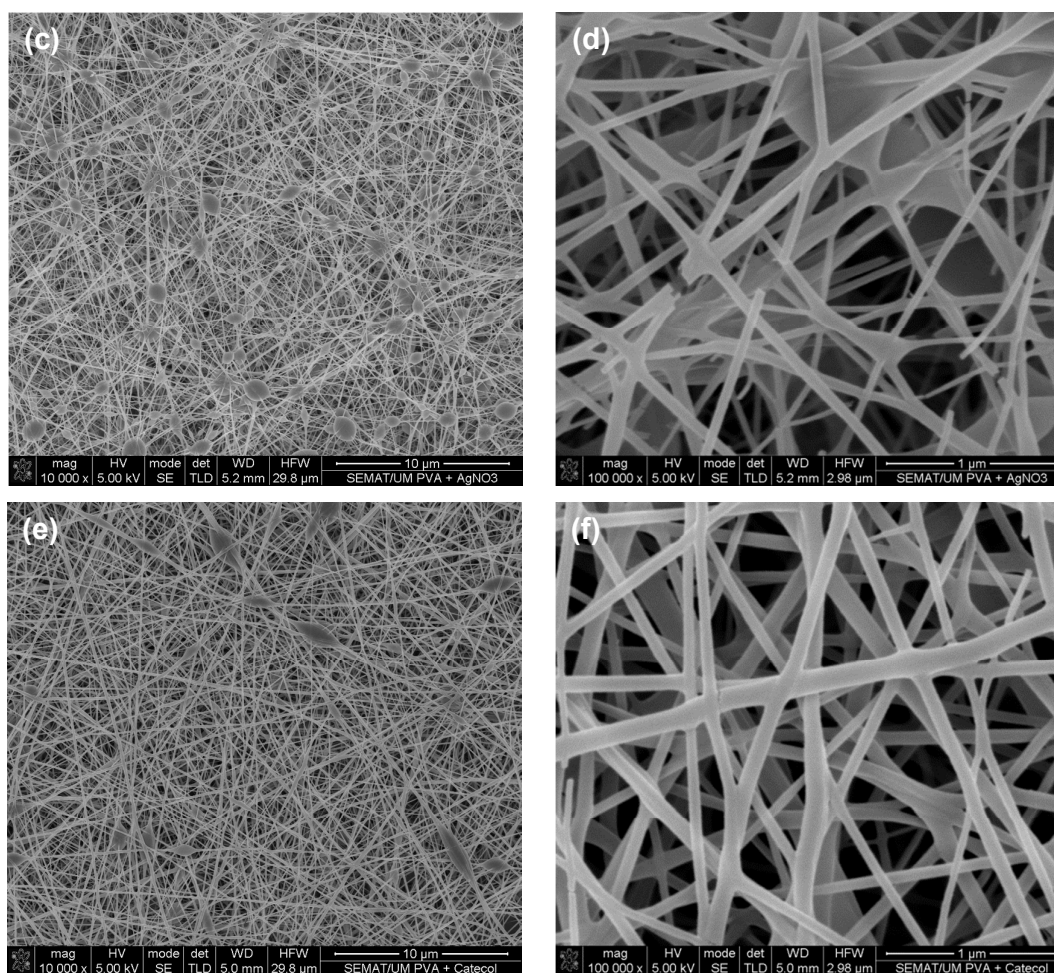
Figure 1 - SEM of the (a, b) PVA nanofibres and PVA blended with (c, d) AgNO$_3$ and (e, f) PC at magnifications x10,000 and x100,000.

Table 1. Porosity and average fiber diameter of the PVA, PVA/AgNO$_3$ and PVA/PC nanofibers electrospun onto a PVDF basal membrane.

| Membranes	Porosity (%)	Fiber Diameter (nm)
PVDF+PVA	87.8	81.4 ± 32.4
PVDF+PVA/AgNO$_3$	90.3	63.8 ± 31.7
PVDF+PVA/PC	51.3	98.2 ± 20.3

By EDS and XPS, the relative atomic composition of the PVA, PVA/AgNO$_3$ and PVA/PC electrospun nanofibers on the PVDF membrane was determined (Table 2, Figure S1 in Supporting Information). As expected, only on the PVA/AgNO$_3$ blend other elements aside from C and O were observed. Here, N and Ag from the AgNO$_3$ were detected confirming an efficient blending. Between the PVA and the PVA/PC blend, as the chemical composition of PVA is (C$_2$H$_4$O)$_n$ and catechol is C$_6$H$_6$O$_2$ and, thus, only C and O can be detected, no significant differences would be expected from this analysis (the condensed formula of the main chemicals used in this investigation can be depicted in Figure S2 in Supporting Information). EDS and XPS techniques differ significantly on the specimen excitation, size of the excitation area (0.5-4 μm of EDS vs. 15-500 μm of XPS), and depth resolution (500-3000 nm of EDS vs. 1-10 nm of XPS). However, since XPS is characterized by a lower planar but a higher vertical resolution than EDS, it is able to create deeper profiles of the chemical structure of the materials. Moreover, XPS analysis is generally free of matrix effects, which is the cause of a lower quantitative accuracy in EDS. The main difference between the two techniques, in this case, is the fact that the amount of Ag observed by XPS is higher with a concomitant lower concentration of the counter ion than the observed by EDS. This suggests a good availability of Ag ions on the surface of the nanofibers (Figure S3 and S4 in Supporting Information).

Table 2. Relative chemical composition and atomic ratio determined by EDS and XPS of PVA, PVA/AgNO$_3$ and PVA/PC nanofibers electrospun onto a PVDF basal membrane.

Membranes	At (%)					Atomic Ratio
	C	O	N	Ag	Imp.	O/C

	PVDF+PVA	62.56	37.06	-	-	0.38	0.59
EDS	PVDF+PVA/AgNO$_3$	53.19	40.42	2.93	3.46	-	0.76
	PVDF+PVA/PC	62.01	36.82	-	-	1.17	0.59
	PVDF+PVA	70.00	30.00	-	-	-	0.43
XPS	PVDF+PVA/AgNO$_3$	66.57	31.38	0.62	1.43	-	0.47
	PVDF+PVA/PC	70.76	29.24	-	-	-	0.41

The XPS high-resolution deconvoluted spectra and the corresponding atomic compositions are shown in Figure 2 and Table 3. Deconvolution of the C1s core level of the PVDF+PVA, PVDF+PVA/AgNO$_3$ and PVDF+PVA/PC show the expected stoichiometric ratios of the individual C components as shown in Table 3. The O1s XPS spectra of the three samples are similar and the ratio of O species is in accordance with the stoichiometric O content for each sample (Table 3). The PVDF+PVA/AgNO$_3$ sample shown a peak in the N1s core at 406.8 eV level typically attributed to the NO_3^- and NO_2^- anions.[30] The Ag 3d$_{5/2}$ component was deconvoluted in three subpeaks, a main peak at 368.6 eV attributed to AgNO$_3$ and two small peaks at higher binding energies attributed to the presence of small amount of nanoparticles formed during the electrospinning procedure. However, no nanoparticles can be observed in the SEM analysis because the electrospun PVA/AgNO$_3$ fibers were not produced with the intent to improve the Ag reduction on the PVA matrix.
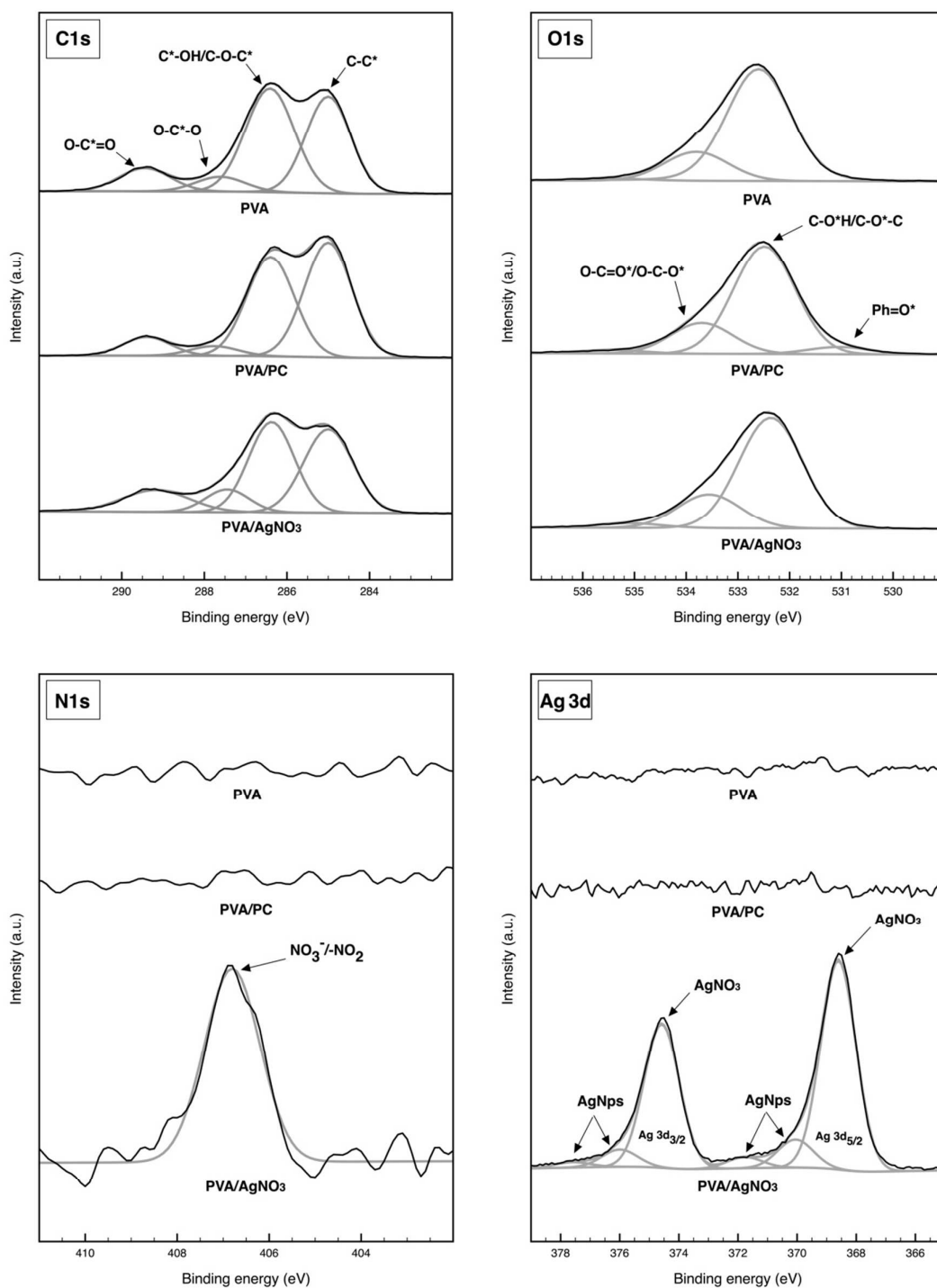
Figure 2 - High-resolution XPS C1s, O1s, N1s and Ag 3d spectra of PVA, PVA/AgNO₃ and PVA/PC nanofibers electrospun onto a PVDF basal membrane.

14

Table 3. Different chemical functional groups and represented by the deconvolution C1s, N1s, O1s and Ag d3 XPS peaks of PVA, PVA/AgNO₃ and PVA/PC nanofibers electrospun onto a PVDF basal membrane.

Binding energy (eV)	Functional group	Relative area of deconvoluted peaks (%)		
		PVDF+PVA	PVDF+PVA/AgNO₃	PVDF+PVA/PC
285.0	C-C*	38.3	38.4	47.3
286.4	C-O*H/C-O-C*	44.8	38.6	41.0
287.6	O-C*-O	6.4	9.3	4.0
289.4	O-C*=O	10.5	13.7	7.7
368.6	Ag $3d_{5/2}$ AgNO₃	-	50.4	-
370.1/371.8	Ag $3d_{5/2}$ AgNPs	-	9.5	-
374.6	Ag $3d_{3/2}$ AgNO₃	-	34.7	-
376.0/377.6	Ag $3d_{3/2}$ AgNPs	-	5.5	-
406.8	NO_3^-/-NO_2	-	100	-
532.5	C-O*H	79.3	74.1	72.2
533.7	O-C=O*/O-C-O*	20.7	25.9	22.9
531.0	Ph=O*	-	-	4.8

TGA analysis of the PVDF, PVA, PVDF+PVA, PVDF+PVA/AgNO₃ and PVDF+PVA/PC membranes (Figure 3) put in evidence three well-differentiated steps of degradation. For all combinations, the first step corresponds to the initial weight loss in water. PVDF sample is very stable until temperatures as high as 400 ºC, after those it begins to degrade with a 70% mass loss, T_{max} at 510 °C. After the main degradation, a second weight loss step occurs and the residue obtained is ≈ 2%, at ≈ 700 ºC. Also in the case of PVA, decomposition occurs mainly in two degradation steps. The first starts at ≈ 300 ºC, T_{max} at 350 °C, representing a loss in mass of ≈ 80%. In the end of step 2, at 500 ºC, only ≈ 5 % of residual mass was observed. By electrospinning PVA or the

15

tested blends onto PVDF the weight loss behavior with time alters. Three well-differentiated steps can be depicted. The first smallest step at $\approx$ 350 ºC corresponds to the PVA nanofibers degradation while the second step at $\approx$ 500 ºC corresponds to the PVDF membrane degradation. The third degradation step evolves at a slower rate and continues until temperature reaches 900 ºC, remaining $\approx$ 38%, $\approx$ 5% and $\approx$ 30% of residual mass on the PVDF+PVA, PVDF+PVA/AgNO$_3$ and PVDF+PVA/PC membranes, respectively.
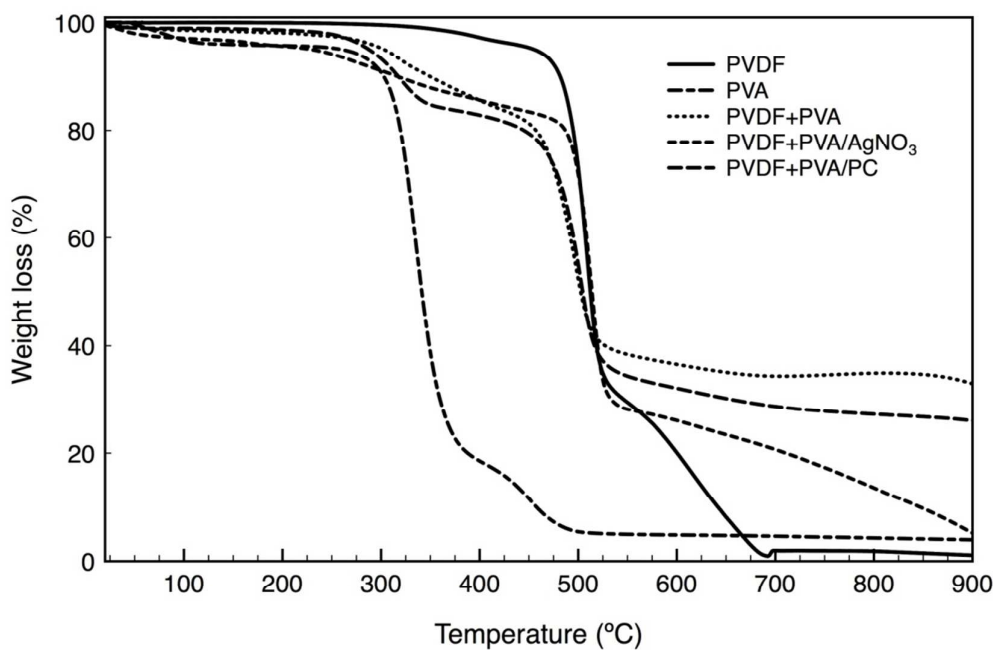
Figure 3 - TGA of the PVDF basal membrane and the PVDF electropsun with PVA, PVA/AgNO$_3$ and PVA/PC nanofibers from 35 °C to 900 °C, performed at a heating rate of 10 °C/min, in a nitrogen atmosphere.

The DSC analysis (Figure 4) detected the melting temperature of PVFD and PVDF+PVA at $\approx$ 158 ºC, the PVDF+PVA/AgNO$_3$ at $\approx$ 161 ºC and the PVDF+PVA/PC

16

membranes at ≈ 159 ºC. As only one peak was detected for each sample, the blends

were recognized as homogeneous. Despite DSC being able to easily recognize the

melting point of the generated composite, it is not always accurate enough in identifying

Tg transitions.
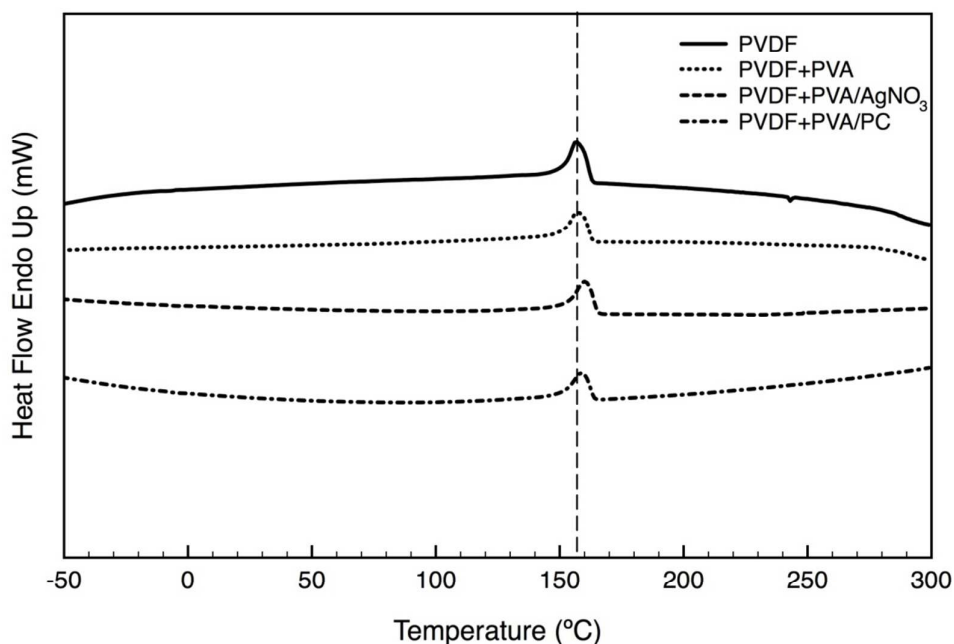
Figure 4 - DSC thermograms of 2nd heating of PVDF basal membrane and the PVDF

electrospun with PVA, PVA/AgNO$_3$ and PVA/PC nanofibres in a temperature range of

-50 to 300 ˚C at 10 ˚C/min.

Since these data was inconclusive, the DMA technique, which is a more sensitive

method in terms of relaxation behavior, was used. Data was reported in terms of loss or

damping factor (tan δ), which relates the loss modulus with the storage modulus and

provides information on the relative contributions of the viscous and elastic components

of a viscoelastic material.[29] The DMA analysis (Figure 5) was conducted on the PVFD,

PVDF+PVA, PVDF+PVA/AgNO$_3$ and PVDF+PVA/PC membranes. Electrospinning of

PVA and its blends was directly done on the PVDF membranes being, therefore, impossible to separate the PVA electrospun layer from the latter and analyze it individually. Four regions with different elastic behavior were detected, two secondary and two main relaxation peaks. The two main relaxation peaks were observed at ≈ 40 ℃ and ≈ 65 ℃, while the secondary were found at ≈ -5 ℃ and ≈ 20 ℃. The Tg peak at 65 ℃ is attributed to PVA and does not appear in the bare PVDF. After the addition of AgNO$_3$ the PVA peak clearly shifted to lower temperatures while PC shifted to higher. It may be difficult to identify precisely a single temperature peak for each sample, still the shift is significant even if the peak is calculated from a range of temperatures in the curve plateau (55-65 ℃ for PVDF+PVA, 65-75 ℃ for PVDF+PVA/PC and 45-55 ℃ for PVDF+PVA/AgNO$_3$). Moreover the PVDF+PVA/PC peak showed a higher tan δ than the other membranes, reducing significantly its elastic modulus (more viscous material).
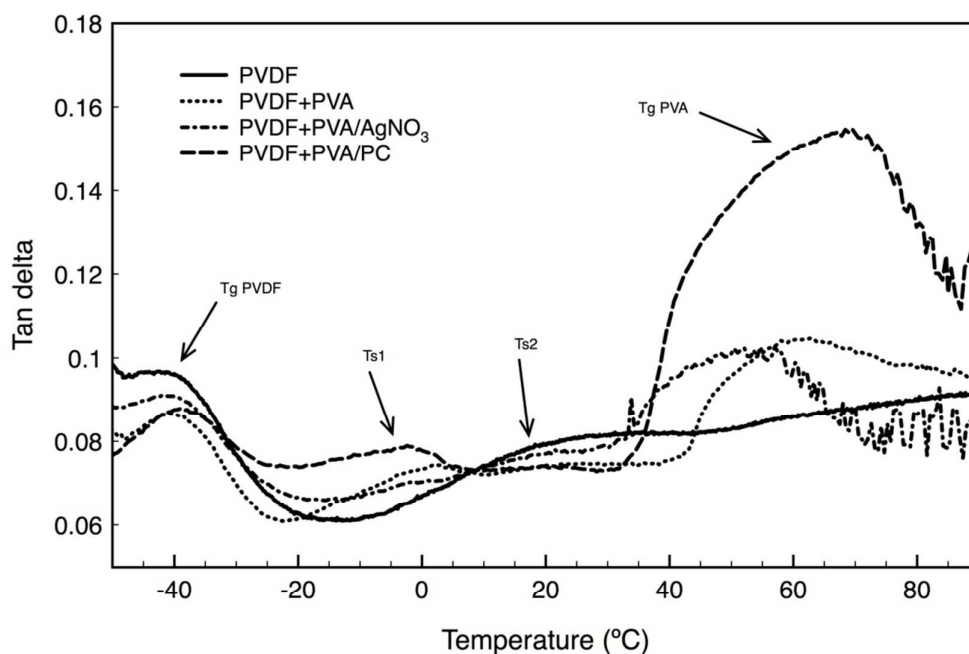
Figure 5 - Tan δ curves versus temperature of the membranes PVDF and PVDF electrospun with PVA, PVA/AgNO$_3$ and PVA/PC nanofibers.

3.2. Antimicrobial Activity. The membranes antimicrobial activity was measured against *E. coli* and *S. aureus* using the standard shake flask method. After 1 h contact, the number of viable microorganisms was counted and the percentage of reduction determined. Data collected (Table 4) established the PVDF+PVA/AgNO$_3$ as the most promising to prevent bacterial immobilization (100% reduction). PVDF+PVA/PC was also very important against *S. aureus* (92% reduction), however was only capable of reducing *E. coli* activity in 13%. PVDF and PVDF+PVA had little to none influence on the bacteria response.

Table 4. Antimicrobial activity of the filtration membranes using *E. coli* and *S. aureus*.

Membranes	Bacterial reduction (%)	
	E. coli	*S. aureus*
PVDF	17%	-2%
PVDF+PVA	-3%	-23%
PVDF+PVA/AgNO$_3$	100%	100%
PVDF+PVA/PC	13%	92%

3.3. Ultrafiltration. The ultrafiltration performance of the developed PVDF+PVA/PC membrane was established by direct measurement of the C.I. Reactive Red 66 monoazo dye in dH$_2$O and synthetic seawater solution at 4 bar. The maximum

removal dye efficiency was determined at $\approx 85\%$ in dH_2O after 5 cycles (Table 5). With

this solution, a relative high filtration flux was also observed. In the presence of salts, a

decrease in both rejection and flux was evidenced. The overall salt rejection was

calculated using a conductivimeter and expressed as percentage reduction using the

seawater mother solution as reference (44 mS cm-1). The results showed an overall salt

reduction of 5% after 5 cycles.

Table 5. Ultrafiltration experiments in Reactive Red 66 dissolved in dH_2O and seawater

using a PVDF membrane electrospun with a PVA/PC.

Solution	Rejection (%)	Flux (L m^{-2} h)	Overall salt rejection (%)
dH_2O	85 ± 2	70 ± 4	-
Seawater	64 ± 2	62 ± 3	5 ± 1

4. DISCUSSION

Electrospinning of single PVA solutions has been reported by many.[31-33] Yet,

combinations of PVA with $AgNO_3$ or PC are less common. The solution parameters,

including concentration, viscosity and conductivity, are determinant to the success of

the final product. For that reason, optimization processes are usually conducted with the

individual polymers prior to the formulation of blends. Since nanofibers could not be

generated from pure $AgNO_3$ or PC solutions, only PVA required further testing. Using

data from a previous work, in which detailed analyses of the effects of different

processing conditions on the formation of PVA nanofibers is given,[29] an optimal

concentration for PVA, suitable even in blends, was established at 12% w/w. Also, it

should be mentioned that because of its solubility in water, PVA-based electrospun nanofibers (in single or blend forms) require an extra step during fabrication. Its unique nanofibrous structure is quickly lost in aqueous environments, becoming inappropriate for water ultrafiltration applications. Crosslinking of PVA polymer with GA is, therefore, necessary to stabilize the electrospun nanofibers. Their morphology, chemical composition and mechanical and thermal properties were then characterized.

Nanofibers resultant from single PVA, PVA/AgNO$_3$ and PVA/PC blends displayed very important features (Figure 1). Presence of beads within the nanofibers and detection of discontinuous and thin nanofibers within the mesh were expected using single PVA due to the low conductivity and viscosity of the solution at 12% w/w.[29] Still, the occurrence of beads and the presence of discontinuous fibers were more prevalent when AgNO$_3$ was present. Beads may stick to fibers changing pore size, they may agglomerate to form larger beads that can obstruct other pores and may also fragilize neighboring nanofibers. It has been reported that the addition of AgNO$_3$ to polymeric solutions increases the charge density in the ejected jets and, thus, stronger elongation forces are imposed, resulting in a morphology change of the e-spun fibers from a bead-on-fiber structure to a uniform fiber structure with straighter shape and smaller diameter.[34-35] Here, however, only the fibers smaller diameter was attained (63.8 ± 31.7 nm, Table 1). The formation of beads was not avoided nor the presence of discontinuous fibers. As the PVA/AgNO$_3$ solution contacts with the metal needle tip and is ejected, Ag oxides are susceptible to be formed and to grow on the surface of the tip forming precipitates that can both difficult the exit of the electrospun solution and lead to the formation of beaded fibers.[36] By combining PC with PVA, formation of beads, thin and discontinuous nanofibers was overcome. The resulting fibers were more homogeneous both in size and shape. Due to its electroactive versatility which allows

PC to undergo a variety of chemical reactions and interact with both organic and inorganic substrates, the repulsive forces between the ionic groups within the polymer backbones may be reduced and, thus, uniform fiber structures can be produced.[1-2] To confirm the homogeneity of the blends and both the presence of $AgNO_3$ and PC on the nanofibers, XPS and EDS analyses were conducted (Table 2). The atomic composition of PVA was found consistent with the literature.[37] Presence of $AgNO_3$ on the $PVA/AgNO_3$ blend was easily demonstrated by the detection of Ag and N at $\approx$ 3% each. As expected, the ratio O/C also increased (more important in the EDS data). The atomic composition of PVA/PC altered very little from single PVA, since both PVA and PC exhibit equal chemical elements (C and O) and the amount of PC added to the blend was not significant enough to alter the O/C ratios. Impurities, most likely resultant from sample handling, were only detected by EDS on PVA and PVA/PC.

The deconvolution of the XPS C1s envelope (Figure 2, Table 3) shows a peak at 285 eV attributed to aliphatic carbon atoms (–C–C–) of the main chain of PVA.[38] The peak at 286.4 eV can be attributed to the C-O-H bond of the hydroxyl group of PVA structure. It is expected that C-O-C groups to be formed between PVA chains during the electrospinning process and after the GA crosslinking.[39] This is confirmed by the presence of the peak at 287.6 eV representing the bond of O-C-O. The oxidation effect of GA on the PVA explains the presence of the peak at 289.4 eV attributed to the carboxyl acid group (O-C=O).[40] The deconvolution of the O1s peak of PVDF+PVA and PVDF+PVA/$AgNO_3$ gave two contributions: the peak at 532.5 eV which is assigned to the C-OH bonds in the PVDF+PVA, and the peak at 533.7 eV which corresponds to the C–OH bond in the carboxylic acid as observed in the C1s core level of the PVDF+PVA.[38, 41] The PVDF+PVA/PC displayed a supplementary peak at 531.0 eV attributed to the carbonyl oxygen of quinones of the catechol oxidized structure.[42]

22

The Ag3d$_{5/2}$ shows the main peak at 368.6 eV that corresponds to AgNO$_3$ proving that most of the metal in the nanofibers is still in the form of salt.[43] The two small peaks at 370.1 and at 371.8 eV suggest the presence of small amount of Ag NPs interacting with the PVA surface.[44] When Ag NPs chemically interacts with polymer moiety a positive shift in binding energy is usually observed.[45-47] As reported, decreasing the size of the Ag NPs leads to an increase in the positive shift of the Ag 3d$_{5/2}$ core electron binding energy.[48] The positive shift in binding energy may be attributed to the size effects (change in the electronic structure) of the noble metals in composite films.[49] The preparation of Ag NPs in an electrospun polymeric matrix is usually achieved by chemical or physical reduction.[50-51] It is important to stress that the main goal of this research was the use of AgNO$_3$ as positive control to establish the antimicrobial efficiency of PVDF+PVA/PC and not to produce nanoparticles. In fact, the electrospinning was performed in a way that the synthesis of nanoparticles was kept to a minimum. Light exposure inevitably creates some reductive conditions which may also explain the presence of silver in the metallic state. The two small peaks suggest the formation of two Ag NPs size distributions lower than 10 nm. This size in addition to the low content could explain the absence of visible NPs in the SEM analysis.

The steps of membrane degradation were defined and characterized by TGA (Figure 3). PVDF was used as commercial control and base substrate for the single PVA, PVA/AgNO$_3$ and PVA/PC electrospun blends. The first step at $\approx$ 100 ºC refers to the initial weight loss resultant from the evolution of moisture from the polymer matrix. However, still less than 10%, this was more important on the PC-containing membrane, suggesting the presence of more water molecules per repeat unit of the polymer. The PVDF membrane starts to degrade at 400ºC continuously until it becomes residual at 700 ºC leading to the formation of hydrogen fluoride, the monomer and small amounts

of $C_4H_3F_3$.[52] Previous reports have shown, the thermal decomposition of pure PVDF to be more important at $\approx$ 500 ºC.[53] Our data is consistent with those findings. The second weight loss step between 500 ºC and 700 ºC may be due to the presence of additives introduced during commercial polymer processing, such as lubricants and plasticizers.[54] PVA decomposition occurs mainly in the second degradation step which starts at $\approx$ 300 ºC, representing a loss in mass of $\approx$ 80%, in which the PVA side chain is lost.[55] The PVA main chain starts degrading after that point[56] and continues throughout step 3, until 900 ºC, at which point only $\approx$ 5 % of residual mass remains. The combination of the tested blends (PVA, PVA/AgNO$_3$ and PVA/PC) with PVDF, alters the thermogravimetric profile of the membrane with time. Indeed, the pattern of degradation only becomes more significant at the second step, after $\approx$ 500 ºC. During step 1, at $\approx$ 350 ºC, degradation refers mostly to PVA, while at step 2 the PVDF membrane is lost. Degradation of PC occurs throughout both the first and second steps. Studies have shown the PC degradation rate to start at $\approx$ 180 ºC and to evolve very slowly with the increase in temperature. As the temperature rises, internal rearrangements of the PC structure occur providing great thermal stability to the catechol units.[10] Still, once reached 900 ºC, $\approx$ 30% of residual mass remains from the PVDF+PVA/PC membrane. The high solid residue content observed at 900 °C might be due to the higher crystalline molecular configuration of the nanofibers containing PVA or to the presence of cations (Na$^+$, K$^+$, Ca^{2+}), which acted like a bridge between different polymer chains.[57] These cations derive from the enzyme preparation which requires several buffers and stabilizers. The presence of silver salt clearly interferes with the nanofibres thermal resistance leading to a slow but gradual mass loss between 550 ºC and 900 ºC. TGA data suggests that the maximum running temperature that can be used during filtration should not exceed 150 ºC since after this value the PVA/PC blend

24

starts degrading. Without considering the high resistance of the PVDF basal membrane, this temperature is a clear improvement over commercially available filtration membranes that stand no more than 100 ºC.

DSC analyses (Figure 4), which established the membranes melting temperatures, provided important information about the homogeneity of the blends. DSC spectra revealed only one endothermic peak, corresponding to the melting point, but did not provide information about the different crystalline phases in which the elements composing the membrane would be found. The PVDF melting temperature was consistent with the literature.[58] Although the melting temperature of PVA ranges 200 ºC,[59] the molecular interactions established with PVDF seems to have decreased its melting point. According to the literature, the melting point of $AgNO_3$ is at $\approx$ 212 ºC and the PC at $\approx$ 125 ºC.[10, 60] The addition of these elements to the PVA blends altered slightly the position of the peaks as new molecular interactions (different from PVDF and single PVA) were formed. However, data acquired from DSC was inconclusive. For that reason, DMA technique was also used (Figure 5). Four regions with different elastic behavior were detected on all tested membranes, two secondary and two main relaxation peaks. The two main relaxation peaks were detected at $\approx$ -40 ºC and $\approx$ 65 ºC and correspond to the glass transition temperatures (Tg) of PVDF and PVA, respectively.[61-62] The Tg peak at 65 ºC was exclusive of PVA and does not appear in the bare PVDF. PVA electrospun nanofibers could not be analyzed individually, since PVA was electrospun directly onto the PVDF membranes, thus making it impossible to separate them. The secondary peaks were found at $\approx$ -5 ºC (T_{s1}) and $\approx$ 20 ºC (T_{s2}) and are associated with the secondary relaxation temperature of PVA and with local molecular motions or conformational changes of the PVA side groups, respectively.[61] After the addition of $AgNO_3$, the PVA peak clearly shifted to lower temperatures, while

PC shifted to a higher. It may be difficult to identify precisely a single temperature peak for each sample, still the shift is significant even if the peak is calculated from a range of temperatures in the curve plateau (55-65 ºC for PVDF+PVA, 65-75 ºC for PVDF+PVA/PC and 45-55 ºC for PVDF+PVA/AgNO$_3$). This happens in response to molecular interactions (hydrogen bonding) that occur between the elements in the blend that promote conformational changes in the structure of the PVA side groups. The same has been reported by Young et al. with chitin and PVA blends, and Sudhamani et al. with Gellan and PVA blends.[59, 63] Also, we have shown chitosan and cyanobacterial extracellular polymeric substances blended with PVA and electrospun onto PVDF surfaces to promote equal effects.[29]

The addition of AgNO$_3$ is responsible for the decrease of the tan δ peak temperature from ≈ 60 ºC to ≈ 50 ºC. This leads to lower interactions between PVA polymer chains and to higher free volume inside the lattice.[64] Despite the shift in temperature, the values of the Tan δ remained very similar. This seems to indicate that the thermoplastic PVA network is not perturbed by the non-thermoplastic inorganic filler (AgNO$_3$) in terms of its viscoelastic properties.[68] The PVDF+PVA/PC peak showed a remarkably higher tan δ and a slightly higher Tg temperature than the other membranes, indicating a significant reduction of its elastic modulus (more viscous material). The shift towards higher Tg could be attributed to the intermolecular interactions between PVA and PC in the form of hydrogen bonding, indicating that the system is very close to being miscible.[65] The DSC and DMA analyses provides important information about the stability of the membrane in terms of operative temperature and pressure. DSC confirmed the TGA data showing that the maximum temperature before filter degradation is about 150 ºC. DMA, which is a more sensitive technique, established that to maintain a constant porosity and consequently promote an effective filtration, it

should be performed between -20 and 30 ºC. This is because after the PVA Tg the nanofibers can be deformed under the ultrafiltration pressure (e.g. 4 bar) changing the pore sizes.

The membranes antimicrobial activity was measured against *E. coli* and *S. aureus* using the standard shake flask method (Table 4). PVDF+PVA/AgNO$_3$ was determined as the most promising to prevent bacterial immobilization (100% reduction), regardless the bacteria type (Gram-positive or Gram-negative). Ag-based compounds are currently being used to control bacterial growth in a variety of applications. They are highly toxic to microorganisms, showing strong biocidal effects on as many as 12 species of bacteria, including *E. coli* and *S. aureus*.[66-67] In addition, Ag-based compounds, like AgNO$_3$, are capable of retaining its effective inhibitory activity against various microorganisms even at very low concentrations,[68] which explains its enhanced performance when blended with PVA and electropsun onto PVDF. PVDF+PVA/PC was also very important against *S. aureus* (92% reduction) but showed a low activity against *E. coli* (13% reduction). PC has also been used as a binding agent to improve the antimicrobial and biocidal features of coatings against *E. coli* and *S. aureus* by orienting its phenyl groups on the substrate surface and promoting an adhesive or cross-linking functionality that discourages leaching and allows the tuning of activity.[4, 27] PC was also reported in literature to display great antibacterial performance against *Pseudomonas putida*, *Pseudomonas pyocyanea* and *Corynebacterual xerosis*, when used individually.[3] To the authors knowledge, this is the first time the antimicrobial features of PC blended with PVA have been tested against *E. coli* and *S. aureus*.

The different behavior for Gram-positive and Gram-negative bacteria may be explained by the differences in the cell walls structure and composition. The cell wall of Gram-positive bacteria is composed of a thick peptidoglycan layer composed of linear

polysaccharide chains cross-linked by short peptides to form a 3D rigid structure. On the other hand, the cell wall of Gram-negative species is more structurally and chemically complex with a thin peptidoglycan layer adjacent to the cytoplasmic membrane and a lipopolysaccharidic outer membrane.[69] The higher antimicrobial resistance of Gram-negative bacteria to PC is related to the hydrophilic surface of the outer membrane and could be also associated with periplasmic-space enzymes capable of degrading molecules introduced from the outside.[70] The enzymes produced in the periplasmic space could be secreted trough the outer membrane reaching the external environment using a type II secretion system or the PC could be able to destabilize the outer membrane allowing the direct access to the periplasmic space enzymes. The absence of membrane bound periplasm in the Gram-positive bacteria allows a higher permeability due to the hydrophilic porous structure of the cell wall that can be easily destabilized by PC or poly(quinones).[71] There are several hypotheses on the antibacterial activity of polyphenols. It has been suggested that polyphenols could inhibit or kill the bacteria physically by direct adsorption onto the surface of the bacterial cell wall. It has also been proposed that oxidative polyphenols could mediate antibacterial activity by the generation of hydrogen peroxide. Yet, so far, there is no consensus concerning these mechanisms.[72]

In a side experiment, an electrospun membrane was also synthesized using resorcinol as precursor instead of catechol. Poly(resorcinol) (PR)-containing membranes showed no antimicrobial activity even though their chemical, morphology and thermo-mechanical properties were similar to those of PC (Figure S5 in Supporting Information). These data revealed the importance of the chemical structure and molecular interactions established between PC and PVA, which may be of extreme importance to gain potent biocidal activity. Because they are not endowed with

antimicrobial properties, PVDF and PVDF+PVA had little to none influence on the bacterial response.

The ultrafiltration capability of the PVDF membranes with assembled PVA/PC electrospun thin-layers was evaluated (Table 5). Maximum removal dye efficiency was established at 85% in dH$_2$O, after 5 cycles. This indicates medium rejection ability, an outcome from the irregular sponge-like thin-layer generated, however with relative high filtration flux. In the presence of salts, a decrease in rejection is observed. This can be explained by the Gibbs-Donnan effect, in which charged particles near a semi-permeable membrane may fail in achieving an evenly distribution across the two sides of the membrane.[73] With time the membranes suffered from flux decline due to its sensitivity to scaling and osmotic pressure that resulted from the presence of salts. In the dead-end filtration, the particles accumulated easily on the top surface of the membranes and form a "cake layer", which reduced the effective pore size of the membrane and increased the resistance to flow with time. The observed flux rates were slightly superior to the commercial TFC membranes ($\approx$ 50 L m-2 h). The overall salt rejection was determined at 5%, after 5 cycles. Typically ultrafiltration salt rejection is not measured, thus comparing these results with commercially available membranes is very difficult. Still, 5% is a remarkable result in view of the high amount of mono-cations present in the seawater solution compared to the average porosity of the basal membrane (0.02 µm). Considering the good filtration rate and rejection performance, the PVDF electrospun membrane with a Gram-positive antimicrobial enzymatically synthesized PVA/PC thin-film has definitely the potential to be considered a candidate for seawater pre-treatment applications, at relatively low cost.

5. CONCLUSION

This study introduced a new mid-layer nanofibrous porous support containing a blend of PVA and PC for thin-film composite membranes used in water ultrafiltration applications. Characterization techniques recognized the electrospun blends as homogeneous, confirmed the presence of both $AgNO_3$ and PC, and established the fashioned membranes as thermally stable. Relevant conformation changes on the PVA structure were observed as the testing temperature raised and additives were combined in blends. PVDF+PVA/$AgNO_3$ membrane exhibited 100% growth inhibition of both Gram-positive and Gram-negative bacteria strains despite its irregular morphology and numerous bead formations. The PVDF+PVA/PC membrane was most effective against *S. aureus* (92%). Contrary to the PVDF+PVA/$AgNO_3$, this membrane revealed a homogeneous morphology with very few bead formations. The ultrafiltration abilities of the membrane PVDF+PVA/PC were tested with dH_2O and seawater. After 5 cycles, a maximum rejection of $\approx$ 85% with an average flux rate of 70 L m^{-2} h^{-1} for dH_2O and $\approx$ 64% with an average flux rate of 62 L m^{-2} h^{-1} for seawater were determined with an overall salt rejection of $\approx$ 5%. The efficacy of this PVDF electrospun membrane with a Gram-positive antimicrobial enzymatically synthesized PVA/PC thin-film has been established and its potential for seawater pre-treatment applications has been demonstrated.

ASSOCIATED CONTENT

Supporting Information.

Wide XPS spectra of PVA, PVA/$AgNO_3$ and PVA/PC nanofibers electrospun onto a PVDF basal membrane were added. Wide XPS spectra of PVDF+PVA/$AgNO_3$ taken in

three different places of the same sample, covering an area of 1 mm^2 each. Condensed

formulas of PVDF, PVA, resorcinol and catechol. EDS spectrum of

PVDF+PVA/AgNO$_3$ taken at a depth probe of 5 μm. TGA, DSC and DMA spectra of

PVDF+PVA/PC and PVDF+PVA/PR membranes. This material is available free of

charge via the Internet at http://pubs.acs.org.

AUTHOR INFORMATION

*Corresponding Author

E-mail: felgueiras.helena@gmail.com

Author Contributions

The manuscript was written with contributions of all authors. All authors have given

approval to the final version of the manuscript.

Notes

The authors declare no competing financial interest.

ACKNOWLEDGMENTS

REFERENCES

1.   Faure, E.; Falentin-Daudré, C.; Jérôme, C.; Lyskawa, J.; Fournier, D.; Woisel, P.; Detrembleur, C., Catechols as Versatile Platforms in Polymer Chemistry. *Prog. Polym. Sci.* **2013,** *38*, 236-270.

2.   Ye, Q.; Zhou, F.; Liu, W., Bioinspired Catecholic Chemistry for Surface Modification. *Chem. Soc. Rev.* **2011,** *40*, 4244-4258.

3.   Kocaçalışkan, I.; Talan, I.; Terzi, I., Antimicrobial Activity of Catechol and Pyrogallol as Allelochemicals. *Z. Naturforsch. C Bio. Sci.* **2006,** *61*, 639-642.

4.   Han, H.; Wu, J.; Avery, C. W.; Mizutani, M.; Jiang, X.; Kamigaito, M.; Chen, Z.; Xi, C.; Kuroda, K., Immobilization of Amphiphilic Polycations by Catechol Functionality for Antimicrobial Coatings. *Langmuir* **2011,** *27*, 4010-4019.

5.   Kobayashi, S.; Uyama, H.; Kimura, S., Enzymatic Polymerization. *Chem. Rev.* **2001,** *101*, 3793-3818.

6.   Kobayashi, S.; Makino, A., Enzymatic Polymer Synthesis: An Opportunity for Green Polymer Chemistry. *Chem. Rev.* **2009,** *109*, 5288-5353.

7.   Kurioka, H.; Uyama, H.; Kobayashi, S., Peroxidase-Catalyzed Dispersion Polymerization of Phenol Derivatives. *Polym. J.* **1998,** *30*, 526-529.

8.   Namekawa, S.; Suda, S.; Uyama, H.; Kobayashi, S., Lipase-Catalyzed Ring-Opening Polymerization of Lactones to Polyesters and its Mechanistic Aspects. *Int. J. Biol. Macromolec.* **1999,** *25*, 145-151.

9.   Dubey, S.; Singh, D.; Misra, R., Enzymatic Synthesis and Various Properties of Poly(catechol). *Enzyme Microb. Technol.* **1998,** *23*, 432-437.

10.   Aktaş, N.; Şahiner, N.; Kantoğlu, Ö.; Salih, B.; Tanyolaç, A., Biosynthesis and Characterization of Laccase Catalyzed Poly(catechol). *J. Polym. Environ.* **2003,** *11*, 123-128.

11.   Kobayashi, S., Enzymatic Polymerization: A New Method of Polymer Synthesis. *J. Polym. Sci. A Polym. Chem.* **1999,** *37*, 3041-3056.

12.   Kobayashi, S.; Shoda, S.-i.; Uyama, H., Enzymatic Polymerization and Oligomerization. In *Polymer Synthesis/Polymer Engineering*, Springer: **1995**, pp 1-30.

13.   Lau, W. J.; Ismail, A. F.; Misdan, N.; Kassim, M. A., A Recent Progress in Thin Film Composite Membrane: A Review. *Desalination* **2012,** *287*, 190-199.

14.   Kim, E.-S.; Kim, Y. J.; Yu, Q.; Deng, B., Preparation and Characterization of Polyamide Thin-Film Composite (TFC) Membranes on Plasma-Modified Polyvinylidene Fluoride (PVDF). *J. Membr. Sci.* **2009,** *344*, 71-81.

15.   Hunley, M. T.; Long, T. E., Electrospinning Functional Nanoscale Fibers: A Perspective for the Future. *Polym. Int.* **2008,** *57*, 385-389.

16.   Chew, S.; Wen, Y.; Dzenis, Y.; Leong, K. W., The Role of Electrospinning in the Emerging Field of Nanomedicine. *Curr. Pharm. Des.* **2006,** *12*, 4751-4770.

17.   Bhardwaj, N.; Kundu, S. C., Electrospinning: A Fascinating Fiber Fabrication Technique. *Biotechnol. Adv.* **2010,** *28*, 325-347.

18.   Halaui, R.; Zussman, E.; Khalfin, R.; Semiat, R.; Cohen, Y., Polymeric Microtubes for Water Filtration by Co−Axial Electrospinning Technique. *Polym. Adv. Technol.* **2016**, *28*, 570-582.

19.   Koski, A.; Yim, K.; Shivkumar, S., Effect of Molecular Weight on Fibrous PVA Produced by Electrospinning. *Mater. Lett.* **2004,** *58*, 493-497.

20.   Taepaiboon, P.; Rungsardthong, U.; Supaphol, P., Drug-Loaded Electrospun Mats of Poly (vinyl alcohol) Fibres and Their Release Characteristics of Four Model Drugs. *Nanotechnology* **2006,** *17*, 2317.

21.   Hong, K. H.; Park, J. L.; Sul, I. H.; Youk, J. H.; Kang, T. J., Preparation of Antimicrobial Poly (vinyl alcohol) Nanofibers Containing Silver Nanoparticles. *J. Polym. Sci. B Polym. Phys.* **2006,** *44*, 2468-2474.

22.   Park, G. Y.; Lee, S. Y.; Kim, W. J.; Choi, J. H. In *Poly (Vinyl Alcohol)(Core)-Polyurethane (Shell) Nanofibers Produced by Coaxial Electrospinning*, Key Engineering Materials, Trans Tech Publ: **2016**; pp 68-71.

23.   Bonino, C. A.; Krebs, M. D.; Saquing, C. D.; Jeong, S. I.; Shearer, K. L.; Alsberg, E.; Khan, S. A., Electrospinning Alginate-Based Nanofibers: From Blends to Crosslinked Low Molecular Weight Alginate-Only Systems. *Carbohydr. Polym.* **2011,** *85*, 111-119.

24.   Charernsriwilaiwat, N.; Rojanarata, T.; Ngawhirunpat, T.; Opanasopit, P., Electrospun Chitosan/Polyvinyl Alcohol Nanofibre Mats for Wound Healing. *Int. Wound J.* **2014,** *11*, 215-222.

25.   Tarun, K.; Gobi, N., Calcium Alginate/PVA Blended Nanofibre Matrix for Wound Dressing. *Indian J. Fibre Text. Res* **2012,** *37*, 127-132.

26.   Yang, J. M.; Yang, J. H.; Tsou, S. C.; Ding, C. H.; Hsu, C. C.; Yang, K. C.; Yang, C. C.; Chen, K. S.; Chen, S. W.; Wang, J. S., Cell Proliferation on PVA/Sodium

Alginate and PVA/Poly (γ-glutamic acid) Electrospun Fiber. *Mater. Sci. Eng. C* **2016,** *66*, 170-177.

27.   Son, H. Y.; Ryu, J. H.; Lee, H.; Nam, Y. S., Silver−Polydopamine Hybrid Coatings of Electrospun Poly (vinyl alcohol) Nanofibers. *Macromol. Mater. Eng.* **2013,** *298*, 547-554.

28.   Tzanov, T.; Silva, C. J.; Zille, A.; Oliveira, J.; Cavaco-Paulo, A., Effect of Some Process Parameters in Enzymatic Dyeing of Wool. *Appl. Biochem. Biotech.* **2003,** *111*, 1-13.

29.   Santos, C.; Silva, C. J.; Büttel, Z.; Guimarães, R.; Pereira, S. B.; Tamagnini, P.; Zille, A., Preparation and Characterization of Polysaccharides/PVA Blend Nanofibrous Membranes by Electrospinning Method. *Carbohydr. Polym.* **2014,** *99*, 584-592.

30.   Zhihui, C.; Rongjie, Y., Study On The In-situ Coating By Octadecylamine of Pyrotechnically Generated Aerosol Particles for Fire Suppression. *Fire Saf. Sci.* **2005,** *8*, 801-809.

31.   Saallah, S.; Naim, M. N.; Lenggoro, I. W.; Mokhtar, M. N.; Bakar, N. F. A.; Gen, M., Immobilisation of Cyclodextrin Glucanotransferase into Polyvinyl Alcohol (PVA) Nanofibres Via Electrospinning. *Biotechnol. Rep.* **2016,** *10*, 44-48.

32.   Lee, K. S.; Eom, K. H.; Lim, J.-H.; Ryu, H.; Kim, S.; Lee, D.-K.; Won, Y. S., Aqueous Boron Removal by Using Electrospun Poly (vinyl alcohol)(PVA) Mats: A Combined Study of IR/Raman Spectroscopy and Computational Chemistry. *J. Phys. Chem. A* **2017,** *121*, 2253-2258.

33.   Long, F.; Kamsom, R.; Nurfaizey, A.; Isa, M.; Masripan, N., The Influence of Electrospinning Distances on Fibre Diameter of Poly (vinyl alcohol) Electrospun Nanofibres. *Proc. MERD* **2017,** *2017*, 377-378.

34.   Jin, W.-J.; Jeon, H. J.; Kim, J. H.; Youk, J. H., A Study on the Preparation of Poly (vinyl alcohol) Nanofibers Containing Silver Nanoparticles. *Synth. Met.* **2007,** *157*, 454-459.

35.   Hang, A. T.; Tae, B.; Park, J. S., Non-Woven Mats of Poly (vinyl alcohol)/chitosan Blends Containing Silver Nanoparticles: Fabrication and Characterization. *Carbohydr. Polym.* **2010,** *82*, 472-479.

36.   Hong, K. H., Preparation and Properties of Electrospun Poly (vinyl alcohol)/Silver Fiber Web as Wound Dressings. *Polym. Eng. Sci.* **2007,** *47*, 43-49.

37.   Louette, P.; Bodino, F.; Pireaux, J.-J., Poly (vinyl alcohol) (PVA) XPS Reference Core Level and Energy Loss Spectra. *Surf. Sci. Spectra* **2005,** *12*, 106-110.

38.   Gu, W.; Liao, L. S.; Cai, S. D.; Zhou, D. Y.; Jin, Z. M.; Shi, X. B.; Lei, Y. L., Adhesive Modification of Indium–tin-oxide Surface for Template Attachment for Deposition of Highly Ordered Nanostructure Arrays. *Appl. Surf. Sci.* **2012,** *258*, 8139-8145.

39.   Wong, K. K. H.; Hutter, J. L.; Zinke-Allmang, M.; Wan, W., Physical Properties of Ion Beam Treated Electrospun Poly(vinyl alcohol) Nanofibers. *Eur. Polym. J.* **2009,** *45*, 1349-1358.

40.   Idage, S. B.; Dumbre, M. D.; Singh, R., Photo-Oxidative Degradation of Nylon 6, 6 Under Accelerated Weathering Study by X-Ray Photoelectron Spectroscopy. *Proc. Recent Adv. Polym. Compos.* **2000,** *1*, 703-707.

41.   Reiche, S.; Blume, R.; Zhao, X. C.; Su, D.; Kunkes, E.; Behrens, M.; Schlögl, R., Reactivity of Mesoporous Carbon Against Water – An In-Situ XPS Study. *Carbon* **2014,** *77*, 175-183.

42.   Ma, C.; Xue, W.; Li, J.; Xing, W.; Hao, Z., Mesoporous Carbon-Confined Au Catalysts with Superior Activity for Selective Oxidation of Glucose to Gluconic Acid. *Green Chem.* **2013,** *15*.

43.   Ferraria, A. M.; Carapeto, A. P.; Botelho do Rego, A. M., X-ray Photoelectron Spectroscopy: Silver Salts Revisited. *Vacuum* **2012,** *86*, 1988-1991.

44.   Sumesh, E.; Bootharaju, M. S.; Anshup; Pradeep, T., A Practical Silver Nanoparticle-Based Adsorbent for the Removal of Hg2+ from Water. *J. Hazard. Mater.* **2011,** *189*, 450-457.

45.   Liu, F.; Cao, Z.; Tang, C.; Chen, L.; Wang, Z., Ultrathin Diamond-like Carbon Film Coated Silver Nanoparticles-Based Substrates for Surface-Enhanced Raman Spectroscopy. *ACS Nano* **2010,** *4*, 2643-2648.

46.   Zanna, S.; Saulou, C.; Mercier-Bonin, M.; Despax, B.; Raynaud, P.; Seyeux, A.; Marcus, P., Ageing of Plasma-Mediated Coatings with Embedded Silver Nanoparticles on Stainless Steel: An XPS and ToF-SIMS Investigation. *Appl. Surf. Sci.* **2010,** *256*, 6499-6505.

47.   Davoudi, Z. M.; Kandjani, A. E.; Bhatt, A. I.; Kyratzis, I. L.; O'Mullane, A. P.; Bansal, V., Hybrid Antibacterial Fabrics with Extremely High Aspect Ratio Ag/AgTCNQ Nanowires. *Adv. Funct. Mater.* **2014,** *24*, 1047-1053.

48.   Shin, H. S.; Choi, H. C.; Jung, Y.; Kim, S. B.; Song, H. J.; Shin, H. J., Chemical and Size Effects of Nanocomposites of Silver and Polyvinyl Pyrrolidone Determined by X-ray Photoemission Spectroscopy. *Chem. Phys. Lett.* **2004,** *383*, 418-422.

49.   Shanmugam, S.; Viswanathan, B.; Varadarajan, T. K., A Novel Single Step Chemical Route for Noble Metal Nanoparticles Embedded Organic-Inorganic Composite Films. *Mater. Chem. Phys.* **2006,** *95*, 51-55.
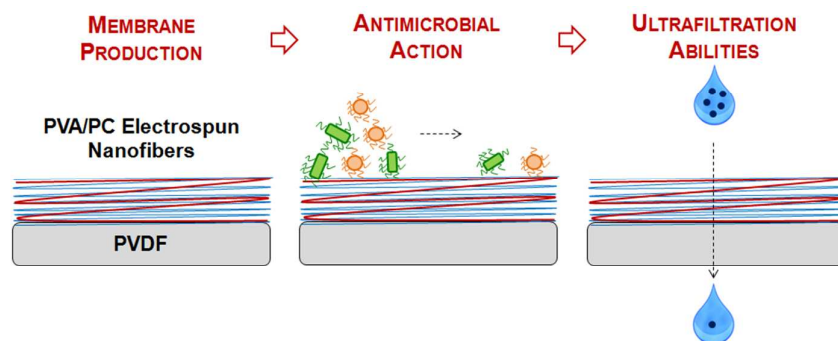
50.   Son, W. K.; Youk, J. H.; Lee, T. S.; Park, W. H., Preparation of Antimicrobial Ultrafine Cellulose Acetate Fibers with Silver Nanoparticles. *Macromol. Rapid Commun.* **2004,** *25*, 1632-1637.

51.   Hong, K. H.; Park, J. L.; Sul, I. H.; Youk, J. H.; Kang, T. J., Preparation of Antimicrobial Poly(vinyl alcohol) Nanofibers Containing Silver Nanoparticles. *J. Polym. Sci. B Polym. Phys.* **2006,** *44*, 2468-2474.

52.   Malmonge, L., Thermal Analysis of Conductive Blends of PVDF and Poly(o-methoxyaniline). *Polymer* **2000,** *41*, 8387-8391.

53.   Bai, H.; Wang, X.; Zhou, Y.; Zhang, L., Preparation and Characterization of Poly (vinylidene fluoride) Composite Membranes Blended with Nano-Crystalline Cellulose. *Prog. Nat. Sci.* **2012,** *22*, 250-257.

54.   Botelho, G.; Lanceros-Mendez, S.; Gonçalves, A. M.; Sencadas, V.; Rocha, J. G., Relationship Between Processing Conditions, Defects and Thermal Degradation of Poly(vinylidene fluoride) in the β-phase. *J. Non-Cryst. Solids* **2008,** *354*, 72-78.

55.   Peng, Z.; Kong, L. X., A Thermal Degradation Mechanism of Polyvinyl Alcohol/Silica Nanocomposites. *Polym. Degrad. Stab.* **2007,** *92*, 1061-1071.

56.   Shao, C.; Kim, H.-Y.; Gong, J.; Ding, B.; Lee, D.-R.; Park, S.-J., Fiber Mats of Poly (vinyl alcohol)/Silica Composite Via Electrospinning. *Mater. Lett.* **2003,** *57*, 1579-1584.

57.   Pooja, K. P.; Chandra, T. S., Production and Partial Characterization of a Novel Capsular Polysaccharide KP-EPS Produced by Paenibacillus pabuli strain ATSKP. *World J. Microb. Biot.* **2009,** *25*, 835-841.

58.   Lanceros-Mendez, S.; Mano, J.; Costa, A.; Schmidt, V., FTIR and DSC Studies of Mechanically Deformed β-PVDF Films. *J. Macrom. Sci. B* **2001,** *40*, 517-527.
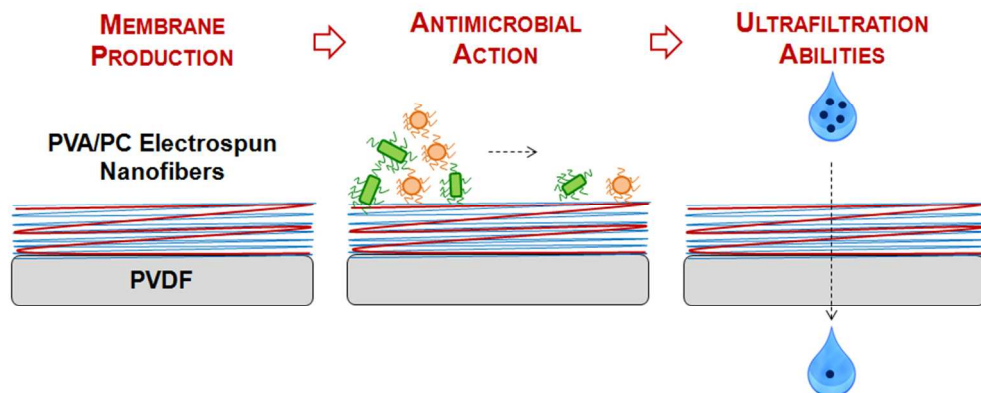
59.   Sudhamani, S.; Prasad, M.; Sankar, K. U., DSC and FTIR Studies on Gellan and Polyvinyl Alcohol (PVA) Blend Films. *Food Hydrocolloid.* **2003,** *17*, 245-250.

60.   Rusu, A.; Popescu, G.-C.; Imre, S.; Ion, V.; Vancea, S.; Grama, A.-L.; Kelemen, H.; Hancu, G., A New Silver Complex with Ofloxacin–Preliminary Study. *AMM* **2016,** *62*, 192-198.

61.   Cassu, S. N.; Felisberti, M. I., Poly (vinyl alcohol) and Poly (vinylpyrrolidone) Blends: 2. Study of Relaxations by Dynamic Mechanical Analysis. *Polymer* **1999,** *40*, 4845-4851.

62.   Gasmi, A.; Gouasmia, M.; Etienne, S. In *Mechanical relaxations and transitions in poly (vinylidene fluoride) PVDF*, Solid State Phenomena, Trans Tech Publ: **2006**; pp 151-156.

63.   Lee, Y. M.; Kimt, S. H.; Kimt, S. J., Preparation and Characteristics of β-chitin and Poly (vinyl alcohol) Blend. *Polymer* **1996,** *37*, 5897-5905.

64.   Mahanta, N.; Valiyaveettil, S., In Situ Preparation of Silver Nanoparticles on Biocompatible Methacrylated Poly(vinyl alcohol) and Cellulose Based Polymeric Nanofibers. *Rsc. Adv.* **2012,** *2*, 11389-11396.

65.   Lee, Y. M.; Kim, S. H.; Kim, S. J., Preparation and Characteristics of Beta-Chitin and Poly(vinyl alcohol) Blend. *Polymer* **1996,** *37*, 5897-5905.

66.   Feng, Q.; Wu, J.; Chen, G.; Cui, F.; Kim, T.; Kim, J., A Mechanistic Study of the Antibacterial Effect of Silver Ions on Escherichia coli and Staphylococcus aureus. *J. Biomed. Mater. Res.* **2000,** *52*, 662-668.

67.   Jung, W. K.; Koo, H. C.; Kim, K. W.; Shin, S.; Kim, S. H.; Park, Y. H., Antibacterial Activity and Mechanism of Action of the Silver Ion in Staphylococcus aureus and Escherichia coli. *Appl. Environ. Microbiol.* **2008,** *74*, 2171-2178.

39

68. Hidalgo, E.; Bartolomé, R.; Barroso, C.; n, o.; Moreno, A.; Domínguez, C., Silver Nitrate: Antimicrobial Activity Related to Cytotoxicity in Cultured Human Fibroblasts. *Skin Pharmacol. Physiol.* **1998,** *11*, 140-151.

69. Lawrence, R.; Tripathi, P.; Jeyakumar, E., Isolation, Purification and Evaluation of Antibacterial Agents from Aloe Vera. *Braz. J. Microbiol.* **2009,** *40*, 906-915.

70. Shan, B.; Cai, Y.-Z.; Brooks, J. D.; Corke, H., The In Vitro Antibacterial Activity of Dietary Spice and Medicinal Herb Extracts. *Int. J. Food Microbiol.* **2007,** *117*, 112-119.

71. Gyawali, R.; Ibrahim, S. A., Natural Products as Antimicrobial Agents. *Food Control* **2014,** *46*, 412-429.

72. Taguri, T.; Tanaka, T.; Kouno, I., Antibacterial Spectrum of Plant Polyphenols and Extracts Depending Upon Hydroxyphenyl Structure. *Biol. Pharm. Bull.* **2006,** *29*, 2226-2235.

73. Nguyen, M. K.; Kurtz, I., Determinants of Plasma Water Sodium Concentration as Reflected in the Edelman Equation: Role of Osmotic and Gibbs-Donnan Equilibrium. *Am. J. Physiol. Renal Physiol.* **2004,** *286*, F828-F837.

Table of Contents Graphic (TOC)

MEMBRANE PRODUCTION ⇨ **ANTIMICROBIAL ACTION** ⇨ **ULTRAFILTRATION ABILITIES**

PVA/PC Electrospun Nanofibers

PVDF

TOC

81x32mm (300 x 300 DPI)